Hadroproduction of four top quarks in the POWHEG BOX

Tomáš Ježo[1,*] and Manfred Kraus[2,†]

[1]*Institut für Theoretische Physik, Westfälische Wilhelms-Universität Münster, Wilhelm-Klemm-Straße 9, 48149 Münster, Germany*

[2]*Physics Department, Florida State University, Tallahassee, Florida 32306-4350, USA*

(Received 26 March 2022; accepted 3 June 2022; published 16 June 2022)

We present a new Monte Carlo event generator for the hadronic production of four top quarks in the POWHEG BOX framework. Besides the dominant next-to-leading order QCD corrections at $\mathcal{O}(\alpha_s^5)$ we also include all subleading electroweak productions channels at leading-order accuracy. We validate our theoretical predictions by comparing to parton-shower matched predictions obtained within the MC@NLO framework for stable top quarks. Furthermore, we investigate in detail the various sources of theoretical uncertainties. Finally, we investigate a single lepton plus jets signature to study for the first time the impact of the electroweak production modes as well as spin-correlation effects at the fiducial level.

DOI: 10.1103/PhysRevD.105.114024

I. INTRODUCTION

Since the discovery of the top quark in 1995 by the CDF [1,2] and DØ [3] experiments at the Tevatron the landscape of top-quark phenomenology has changed dramatically. With the advent of the Large Hadron Collider (LHC) top-quark pairs are so abundantly produced that the top-quark physics program has entered the precision era. Due to its high center-of-mass energy, the LHC offers the unique possibility to produce directly final states involving multiple heavy particles. Thus, in recent years the LHC experiments were able to measure the associated production of top-quark pairs with gauge bosons (W, Z, γ) [4–7] culminating in the discovery of the $t\bar{t}H$ production process [8,9].

However, there is one rare production process that is of particular interest but for which a discovery has not been claimed so far: the production of four top quarks, $pp \to t\bar{t}t\bar{t}$, which can only be produced in very high energetic collisions, due to the large threshold of $\sqrt{s} \sim 700$ GeV. Searches for this process have been conducted by both the ATLAS [10,11] and the CMS [12–16] collaborations already for quite some time. In the recent ATLAS measurement [17] of the cross section an observed (expected) significance with respect to the background-only hypothesis of 4.7 (2.6) standard deviations has been reported.

In recent years, a lot of attention has been devoted to the four top-quark final state as its cross section can be significantly modified by possible physics beyond the Standard Model (BSM) [18–27]. For instance, in supersymmetric theories the signal is enhanced by cascade decays of gluino-pair production [28–31]. Due to the large Yukawa coupling y_t of the top quark, the production of the $pp \to t\bar{t}t\bar{t}$ process is also of high importance to study modifications of the Higgs sector. For example, the production of heavy Higgs bosons in association with top-quark pairs in two-Higgs-doublet models [32–34] can have a big impact on this production rate. Similar effects have been also found in certain top-philic dark matter models [35,36]. Furthermore, in some composite-Higgs models the top quark is not a fundamental particle and its compositeness can be studied at lower energies via the impact of higher-dimensional operators of an effective field theory and to which the $pp \to t\bar{t}t\bar{t}$ process is particularly sensitive [37–39].

Given the strong sensitivity of the four top-quark production process to modifications of the Standard Model (SM) dynamics, a measurement of this process can also provide stringent constraints on four-fermion operators if interpreted within an effective field theory approach [39–43] or within simplified models [44,45]. However, the former should be taken with care in the presence of on-shell intermediate resonances [46]. Finally, the four top-quark final state can also be utilized to determine CP properties of the SM Higgs boson [47,48].

In summary, even though the production of four top-quark events is one of the rarest and most energetic signatures at the LHC, it represents an extremely versatile process for testing the consistency of the SM and put further constraints on BSM physics. Nonetheless, top

*tomas.jezo@uni-muenster.de
†mkraus@hep.fsu.edu

quarks are short-living unstable particles that decay predominantly into a W boson and a bottom quark giving rise to a $W^+W^-W^+W^-b\bar{b}b\bar{b}$ final state. After accounting for the decays of the W bosons the $t\bar{t}t\bar{t}$ final state yields signatures of unprecedented complexity with at least 12 final state particles, which typically comprise four b jets and additional light jets or multiple leptons. Therefore, in order to harness the full potential of the $pp \to t\bar{t}t\bar{t}$ production process, reliable theoretical predictions for the SM process are necessary.

The dominant next-to-leading order (NLO) QCD corrections at $\mathcal{O}(\alpha_s^5)$ have been calculated in Ref. [49] for the first time and later revised in Ref. [50]. The complete NLO corrections including electroweak (EW) corrections as well as all subleading contributions to the $t\bar{t}t\bar{t}$ production process at perturbative orders from $\mathcal{O}(\alpha^5)$ to $\mathcal{O}(\alpha_s^5)$ have been computed for the first time in Ref. [51]. Furthermore, a comparison of parton shower matched computations in the MC@NLO [52,53] framework as provided by MG5_aMC@NLO [54,55] and SHERPA [56,57] has been presented in Ref. [58].

In this paper we present a state-of-the-art Monte Carlo event generator implemented in the POWHEG BOX V2 framework [59,60]. We consider next-to-leading QCD corrections for the $pp \to t\bar{t}t\bar{t}$ production at $\mathcal{O}(\alpha_s^5)$, while also including all subleading EW production modes at leading-order (LO) accuracy. Furthermore, we model top-quark decays at LO while retaining spin-correlation effects. Having multiple event generators at hand allows to study in more detail various sources of theoretical uncertainties intrinsic to the different approaches of matching fixed-order NLO QCD calculations to parton showers. Our generator is publicly available on the POWHEG BOX website.[1]

The paper is organized as follows. In Sec. II we provide a brief overview of the technical aspects of this work together with a short review of the structure of higher-order corrections for the four top-quark production at hadron colliders. Next, we discuss in Sec. III the numerical setup for the theoretical predictions shown in Sec. IV. At last, we will give our conclusions in Sec. V.

II. TECHNICAL ASPECTS

In this section we introduce our new event generator and elaborate on the technical aspects of its implementation in the POWHEG BOX framework. Before doing so, we review the general structure and importance of the various higher-order corrections at the one-loop level.

A. Anatomy of higher-order corrections to $pp \to t\bar{t}t\bar{t}$

We start by reviewing the findings of Ref. [51] to motivate our choice to also include a subset of the most important subleading contributions. At tree-level the $pp \to t\bar{t}t\bar{t}$ process receives contributions at various orders of the strong (α_s) and electromagnetic (α) coupling. Therefore, the perturbative expansion of the leading-order cross section takes the form

$$\begin{aligned}\sigma_{t\bar{t}t\bar{t}}^{\mathrm{LO}} &= \alpha_s^4\Sigma_{4,0} + \alpha_s^3\alpha\Sigma_{3,1} \\ &\quad + \alpha_s^2\alpha^2\Sigma_{2,2} + \alpha_s\alpha^3\Sigma_{1,3} + \alpha^4\Sigma_{0,4} \\ &= \Sigma_1^{\mathrm{LO}} + \Sigma_2^{\mathrm{LO}} + \Sigma_3^{\mathrm{LO}} + \Sigma_4^{\mathrm{LO}} + \Sigma_5^{\mathrm{LO}}, \end{aligned} \tag{1}$$

where Σ_1^{LO}, Σ_3^{LO}, and Σ_5^{LO} correspond to squared amplitude contributions and are therefore strictly positive. In Fig. 1, we depict a few sample Feynman diagrams for these contributions. On the contrary, the terms Σ_2^{LO} and Σ_4^{LO} originate mostly from the interference of Feynman diagrams from different perturbative orders, for the gg and $q\bar{q}$ initial states, and thus are not necessarily positive. Furthermore, they receive contributions from photon initiated processes.

An atypical feature of the $pp \to t\bar{t}t\bar{t}$ process is the presence of both the $q\bar{q}$ and the gg initiated production channels in the EW contributions up to $\mathcal{O}(\alpha_s^2\alpha^2)$. The subleading terms at $\mathcal{O}(\alpha_s\alpha^3)$ and $\mathcal{O}(\alpha^4)$ contribute only to $q\bar{q}$ channels. The size of these EW contributions has been studied in Ref. [51], where it has been found that the Σ_2^{LO} and Σ_3^{LO} contributions can be as large as -30% and $+40\%$ respectively relative to the leading term, Σ_1^{LO}. The large contributions stem from the $tt \to tt$ scattering, for which a representative Feynman diagram is shown in the middle panel of Fig. 1. The exchange of massive bosons, such as the Higgs or Z boson, between nonrelativistic top quarks gives rise to Sommerfeld enhancements, which have been thoroughly studied for top-quark pair production in Refs. [61,62]. Contrarily, the terms Σ_4^{LO} and Σ_5^{LO} only give rise to corrections below 1%. Even though, some of these, formally subleading, contributions can be very large the total correction amounts to roughly positive 5%–15% depending on the chosen renormalization scale as there are strong cancellations among them.

At the next-to-leading order the situation becomes rather complex and the perturbative expansion of the cross section ranges from $\mathcal{O}(\alpha^5)$ to $\mathcal{O}(\alpha_s^5)$:

$$\begin{aligned}\sigma_{t\bar{t}t\bar{t}}^{\mathrm{NLO}} &= \alpha_s^5\Sigma_{5,0} + \alpha_s^4\alpha\Sigma_{4,1} + \alpha_s^3\alpha^2\Sigma_{3,2} \\ &\quad + \alpha_s^2\alpha^3\Sigma_{2,3} + \alpha_s\alpha^4\Sigma_{1,4} + \alpha^5\Sigma_{0,5}. \end{aligned} \tag{2}$$

As all LO production channels are nonvanishing the classification into pure QCD and pure EW corrections breaks down. The complexity of the computation of NLO corrections in this case increases tremendously because QCD and QED infrared singularities have to be subtracted simultaneously. Only the $\mathcal{O}(\alpha_s^5)$ contribution can be considered a pure QCD correction and represents the bulk of the NLO corrections. The sum of all subleading NLO corrections is below 5% at the inclusive level. However,

[1] https://powhegbox.mib.infn.it.

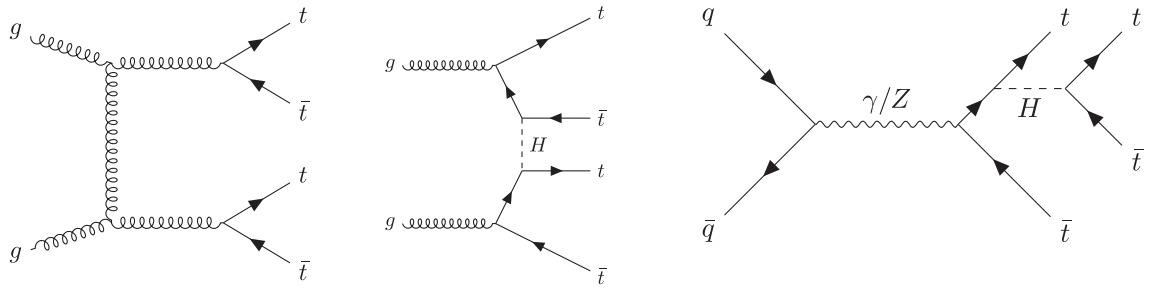

FIG. 1. Representative Feynman diagrams for the tree-level amplitudes at $\mathcal{O}(\alpha_s^2)$ (left), $\mathcal{O}(\alpha_s\alpha)$ (middle), $\mathcal{O}(\alpha^2)$ (right).

partial contributions can be sizable as they compensate for the large scale dependence at the leading order. At the differential level NLO corrections to EW channels can become sizable nonetheless, as demonstrated in Ref. [51], especially in the threshold region. In this region, however, we expect the results based on a fixed-order calculation to be less reliable due to the appearance of large logarithms that ultimately need to be resummed. At future colliders operating at higher energies the subleading EW corrections contribute at the same level to inclusive cross sections, while their relative contributions for differential observables can be much more important if these are sensitive to the threshold region.

In summary, besides the NLO QCD corrections at $\mathcal{O}(\alpha_s^5)$, the dominant contribution for the production of four top quarks are the subleading production channels at LO that amount to roughly a $+10\%$ correction followed by the remaining NLO corrections. The theoretical uncertainties due to the renormalization and factorization scale dependence are also dominated by the leading NLO QCD corrections. In this work we consider NLO QCD corrections and the subleading EW production channels but not the higher-order corrections to those channels. Furthermore, we neglect photon initiated processes as their contributions are suppressed by the photon parton distribution function. In view of the complexity and size of NLO EW corrections we deem them as dispensable for now. Their inclusion will be beneficial at a later stage as they are expected to reduce the theoretical uncertainties of the subleading contributions here included at LO accuracy.

B. Implementation and validation

We proceed with the implementation details and cross checks that we performed to validate our calculation.

The POWHEG BOX framework already provides all process independent ingredients for computing NLO QCD corrections. The necessary tree-level and one-loop matrix elements at $\mathcal{O}(\alpha_s^4)$ and $\mathcal{O}(\alpha_s^5)$ are taken from OpenLoops2 [63–65], which also provides the necessary spin- and color-correlated born matrix elements to construct the infrared subtraction terms. We are using the OpenLoops2 interface to POWHEG BOX introduced in Ref. [66]. The matrix elements for the subleading leading-order electroweak contributions for the $gg \to t\bar{t}t\bar{t}$ and $q\bar{q} \to t\bar{t}t\bar{t}$ processes are instead extracted from MG5_aMC@NLO. Technically, they are included as part of the virtual corrections and, therefore, do not affect the generation of radiation in the POWHEG BOX framework. Neither are they considered in the generation of the color assignment of the underlying born event. This is expected to have a very limited impact, because the EW contributions do not introduce any new basis elements in the colorflow decomposition of the tree-level matrix elements. Thus, our approach is an approximation that treats the subleading EW contributions as an inclusive correction applied to the leading QCD matrix elements. We have confirmed the validity of this approximation by an explicit leading-order parton-shower matched computation using full tree-level matrix elements but assigned colorflows either according to the QCD or the full matrix elements. We found very good agreement between these two options with differences smaller than 2% at the differential level.

The decays of the top-quarks are included using the algorithm presented in Ref. [67], which retains spin correlations at leading-order accuracy. On the technical side, the implementation is a straightforward adaptation of the algorithm used in Ref. [68], which also allows to include off-shell virtualities for resonant particles. For more details on the decay implementation, we refer the reader to the aforementioned references. All necessary QCD decay-chain matrix elements are also taken from MG5_aMC@NLO. Again, we have checked explicitly at leading-order that the structure of the EW contributions, does not modify the spin-correlations effects in the top decay.

We have validated our implementation by performing several cross checks. For instance, we compared all tree-level and one-loop matrix elements against MG5_aMC@NLO at a few phase space points. At fixed-order we reproduced the inclusive cross sections at NLO QCD as given in Ref. [49] and Ref. [51]. The integrated leading-order cross section including all electroweak production channels, as given by Eq. (1), has been checked against Helac-Phegas [69–71]. And finally, the algorithm for the decay of the four top final state has been validated at the differential level against MG5_aMC@NLO in conjunction with MadSpin [72]. To be precise, we compared leptonic observables in the fully

leptonic decay channel at LO accuracy, ignoring the EW tree-level contributions for a moment. We find excellent agreement in all cases once spin correlations have been taking into account.

III. COMPUTATIONAL SETUP

We consider the production of four top-quarks at the LHC with a center-of-mass energy of $\sqrt{s} = 13$ TeV. For this study we fix the SM parameters to the following values

$$\begin{aligned} &G_F = 1.166378 \times 10^{-5}\ \text{GeV}^{-2}, \qquad M_t = 172.5\ \text{GeV}, \\ &M_W = 80.385\ \text{GeV}, \qquad \Gamma_W = 2.09767\ \text{GeV}, \\ &M_Z = 91.1876\ \text{GeV}, \qquad \Gamma_Z = 2.50775\ \text{GeV}, \\ &M_H = 125\ \text{GeV}, \qquad \Gamma_H = 0.00407\ \text{GeV}. \end{aligned} \tag{3}$$

The electromagnetic coupling is derived from the input parameters in the G_μ-scheme [73] and given by

$$\alpha = \frac{\sqrt{2}}{\pi} G_F M_W^2 \left(1 - \frac{M_W^2}{M_Z^2}\right). \tag{4}$$

We calculate the top-quark width at NLO accuracy from all the other input parameters by computing the three-body decay widths $\Gamma(t \to f\bar{f}'b)$ into any light fermion-pair $f\bar{f}'$ and a massive b quark. To this end, we employ a numerical routine of the MCFM implementation of Ref. [74]. If not explicitly mentioned otherwise all presented results have been obtained for the NNPDF3.1 [75][2] parton distribution function (PDF) as provided through the LHAPDF interface [76]. We adopt the dynamical scale choice of Ref. [50] and choose for the renormalization and factorization scale

$$\mu_R = \mu_F = \mu_0 = \frac{H_T}{4}, \tag{5}$$

where

$$H_T = \sum_{i \in \{t,\bar{t},t,\bar{t},j\}} \sqrt{m_i^2 + p_{T,i}^2}\,. \tag{6}$$

In order to estimate the theoretical uncertainty due to our particular choice of renormalization and factorization scales, we vary them independently in the range of

$$\begin{aligned} \left(\frac{\mu_R}{\mu_0}, \frac{\mu_F}{\mu_0}\right) = \{&(0.5, 0.5), (0.5, 1), (1, 0.5), \\ &(1, 1), (1, 2), (2, 1), (2, 2)\}, \end{aligned} \tag{7}$$

and take the envelope as the uncertainty estimate. Let us note, that we vary these scales only in the calculation of the hard matrix elements, thus neither the generation of the hardest emission nor the consecutive parton shower evolution are directly affected by these variations.

The matching in the POWHEG BOX framework depends on the two damping parameters h_{damp} and h_{bornzero} that split the real matrix elements into a finite and an infrared singular contribution. While the singular piece is used to resum soft and collinear QCD splittings the finite part, containing only hard emissions, is treated at fixed-order. For more details on these parameters we refer the reader to Refs. [60,77–79]. Based on experience drawn from previous work [68,79,80] these parameters are chosen as

$$h_{\text{damp}} = \frac{H_T}{4}, \qquad h_{\text{bornzero}} = 5, \tag{8}$$

and h_{damp} is evaluated on the underlying Born kinematics. We study the impact of our choice by considering the envelope of the following independent variations of these parameters

$$\begin{aligned} (h_{\text{damp}}, h_{\text{bornzero}}) = \Big\{&\left(\frac{H_T}{4}, 5\right), \left(\frac{H_T}{4}, 2\right), \\ &\times \left(\frac{H_T}{4}, 10\right), \left(\frac{H_T}{8}, 5\right), \left(\frac{H_T}{2}, 5\right)\Big\}. \end{aligned} \tag{9}$$

As part of the validation of our computation, we perform a comparison of our results with those obtained with the MG5_aMC@NLO framework that employs the MC@NLO matching to parton showers. We use the same input parameters and renormalization and factorization scales as discussed above. Furthermore, the matching in the MC@NLO scheme depends crucially on the choice of the initial shower scale μ_Q. Here we keep the MG5_aMC@NLO default choice of

$$\mu_Q = \frac{H_T}{2}. \tag{10}$$

We study the dependence on this scale by varying it by a factor of 2 up and down.

Finally, for all of the following theoretical predictions we use PYTHIA8 [81,82] (v.8.306) to perform the shower evolution. However, effects from matrix element corrections to the decays, hadronization and multiple interactions are not addressed in this work. The showered events are analyzed using the RIVET [83,84] framework. In the Supplemental Material [85] included with this document we provide the necessary files to reproduce our results. In addition, we provide the numerical data for all shown plots.

IV. PHENOMENOLOGICAL RESULTS

In this section we present our theoretical predictions. We start by investigating the different sources of theoretical uncertainties as well as the impact of subleading EW

[2]The LHAPDF ID numbers for the PDF sets are 315200 at LO and 303400 at NLO.

TABLE I. Total cross sections for the $pp \to t\bar{t}t\bar{t}$ process at $\sqrt{s} = 13$ TeV for the LHC. Cross sections at LO and NLO for various PDF sets are shown together with theoretical uncertainties estimates from scale variations and internal PDF uncertainties.

PDF	$\sigma^{\mathrm{LO}}_{\mathrm{QCD}}$ [fb]	σ^{LO} [fb]	δ_{scale}	σ^{NLO} [fb]	δ_{scale}	δ_{PDF}	$\mathcal{K} = \frac{\mathrm{NLO}}{\mathrm{LO}}$
NNPDF3.1	8.31	8.79	$^{+6.07\ (69\%)}_{-3.30\ (38\%)}$	11.65	$^{+1.98\ (17\%)}_{-2.57\ (22\%)}$	$^{+0.28\ (2\%)}_{-0.28\ (2\%)}$	1.33
MMHT	10.69	11.19	$^{+8.23\ (74\%)}_{-4.36\ (39\%)}$	11.62	$^{+1.95\ (17\%)}_{-2.54\ (22\%)}$	$^{+0.63\ (5\%)}_{-0.53\ (5\%)}$	1.04
CT18	10.04	11.04	$^{+7.68\ (70\%)}_{-4.18\ (38\%)}$	11.74	$^{+1.97\ (17\%)}_{-2.56\ (22\%)}$	$^{+0.46\ (4\%)}_{-0.36\ (3\%)}$	1.06

contributions for the four top-quark production at the inclusive level, i.e., for stable top quarks. Afterwards, we present a sample study for decayed tops in the single-lepton decay channel with a particular focus on the impact of spin correlations contributions at the differential level.

A. Total cross sections

We start our discussion with a detailed investigation of the uncertainty budget of inclusive cross sections. In Table I we show the integrated cross sections at LO accuracy for the leading QCD contribution in the first column and the same also including subleading EW channels in the second column. In the fourth column predictions where NLO QCD corrections on top of the full LO contributions are taken into account are shown. Besides our default choice (NNPDF3.1), we also report integrated cross sections for the MMHT 2014 [86] and CT18 [87] PDF sets. In addition, we also provide the corresponding theoretical uncertainties from scale variations, denoted with δ_{scale} and internal PDF uncertainties denoted with δ_{PDF}. The size of the subleading EW contributions ranges from $+5\%$ to $+10\%$ depending on the PDF set employed, where for MMHT they have the smallest impact and for CT18 the largest. At leading order the scale uncertainties are large and of the order of 70%, which easily accounts for the differences between predictions based on different PDF sets. Including NLO QCD corrections reduces the scale uncertainties by more than a factor of 2 to 22%. The $\mathcal{K}$-factor strongly depends on the PDF set employed at the leading order. For instance, if LO PDF sets are used we find $+33\%$ corrections in the case of the NNPDF PDF set and only between $+4\% - 6\%$ corrections for MMHT and CT18. However, when NLO PDF sets are used for both, LO and NLO predictions, we find a rather large $\mathcal{K}$-factor equal to 1.54 stable with respect to the choice of PDF set. Note that the latter $\mathcal{K}$-factor enters the calculation of the Sudakov form factor of the hardest emission. In view of its large size the necessity of including higher order corrections in fixed order as well as parton-shower matched predictions becomes apparent. The PDF uncertainties are much smaller than the scale uncertainties and have been estimated to be $\pm 2\%$ up to $\pm 5\%$ depending on the chosen PDF set. Let us note here, that we follow Ref. [88] and rescale the PDF uncertainties of the CT18 PDF set, which are provided at the 90% confidence level (CL), by a factor of $1/1.645$ in order to make them comparable with the other PDF sets that provide uncertainties only at the 68% CL. Finally, we also observe that once NLO QCD corrections are taken into account differences for the central prediction for each PDF are at the 1% level, while there are sizable differences at LO.

B. Inclusive differential distributions

Let us now turn to the discussion of differential distributions at the fully inclusive level, i.e., for stable top quarks. We do not impose any selection cuts on the final state top quarks. Jets are defined via the anti-k_T jet algorithm [89] with $R = 0.4$ as provided by FastJet [90,91] and subject to the following cuts

$$p_T(j) > 25\ \mathrm{GeV}, \qquad |y(j)| < 2.5. \tag{11}$$

Furthermore, we order top quarks, irrespective of them being particle or antiparticle, according to their transverse momenta in decreasing order.

Differential cross section distributions are shown in the following as plots containing three panels. The upper panel shows theoretical predictions at NLO accuracy, the middle panel depicts scale uncertainties computed from an envelope of independent variations of renormalization and factorization scales, and the bottom panel illustrates matching uncertainties estimated by varying the various POWHEG BOX specific damping parameters or the initial shower scale μ_Q in the case of the MC@NLO matching scheme in MG5_aMC@NLO. All theoretical predictions including NLO QCD corrections are labeled with *QCD*, while we label predictions that include EW Born contributions as *QCD+EW*. Furthermore, we do not show theoretical uncertainties for the QCD-only predictions obtained with the POWHEG BOX as we find that they are very similar to those when EW contributions are taken into account. Note that even though the subleading EW channels have separately a sizable scale dependence due to $\alpha_s^n(\mu_R)$ with $n \leq 3$, the sum of all EW production modes has a reduced dependence and is smaller than the corresponding scale uncertainty of the dominant NLO QCD corrections at $\mathcal{O}(\alpha_s^5)$.

For the transverse momentum of the hardest top quark shown on the left of Fig. 2, we find very good agreement

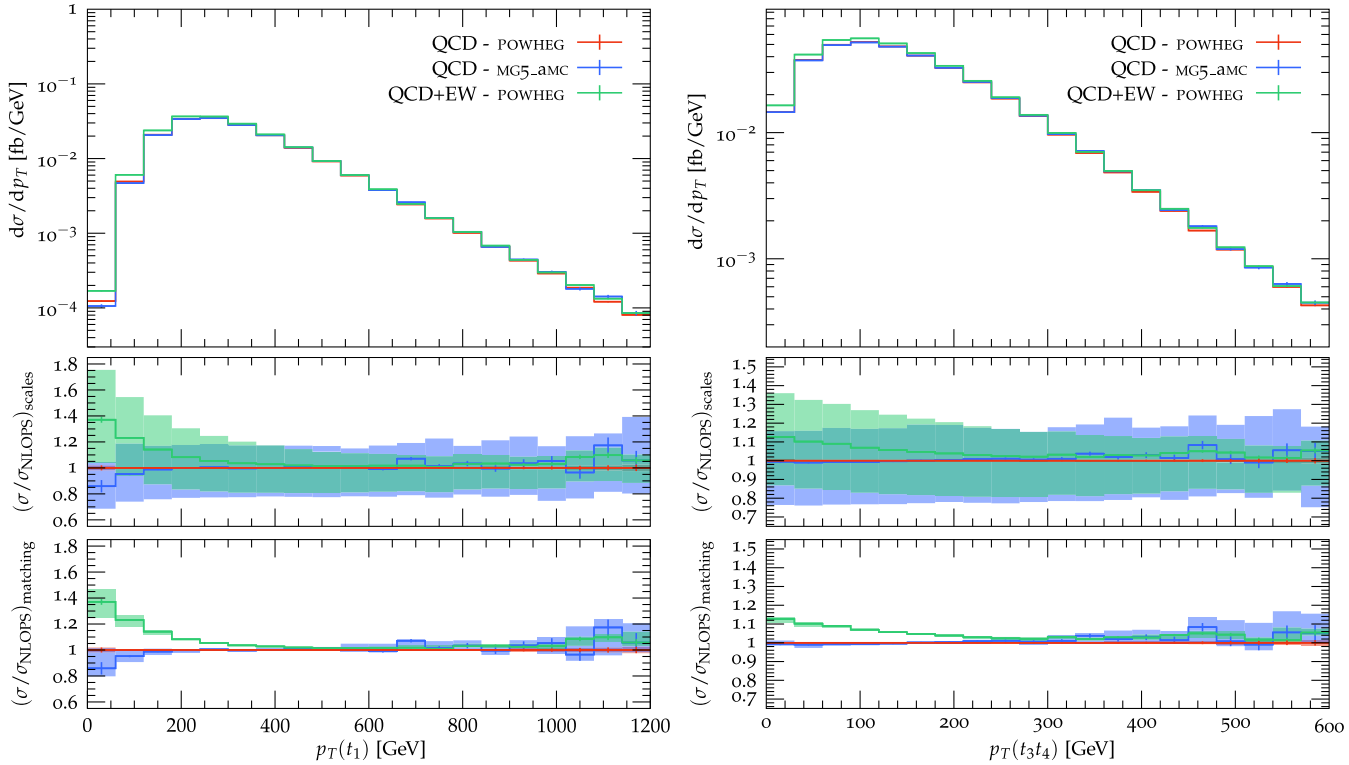

FIG. 2. Differential cross section distribution as a function of the transverse momentum of the hardest top quark (left) and of the third and fourth hardest top-quark pair (right) for the $pp \to t\bar{t}t\bar{t}$ process. The uncertainty bands correspond to independent variations of the renormalization and factorization scales (middle panel) and of the matching parameters (bottom panel).

between MG5_aMC@NLO and the QCD only prediction of POWHEG BOX. Only in the threshold region, where the transverse momenta of all four top quarks become small, differences at the level of 15% are visible. However, this phase space region is also subject to sizable matching uncertainties of the order of 10% for all predictions. In addition, we observe that the EW LO processes give rise to sizable corrections in the threshold region of up to nearly +40%. However, for transverse momenta larger than 300 GeV the EW contributions modify the spectrum by less than 3%. For all theoretical predictions the scale uncertainties due to missing higher-order corrections are the dominant source of uncertainty over the whole range of the distribution. In the case of MG5_aMC@NLO they range from ±20% in the threshold region to ±30% in the tail of the distribution. In POWHEG BOX, the uncertainties are slightly smaller and their pattern is inverted ranging from ±28% at the beginning of the plotted spectrum to ±15% at the end. We checked explicitly that the increased scale dependence in the threshold region is not due to the inclusion of the EW contributions at leading order accuracy. Therefore, the differences should be rather associated to the different matching frameworks.

Let us now turn to the transverse momentum of the combined third and fourth hardest top quark depicted in the right panel of Fig. 2. Here we find a remarkable agreement between MG5_aMC@NLO and POWHEG BOX over the whole plotted range if only QCD contributions are taken into account. However, also here we observe sizable corrections of +12% from the EW contributions for small values of the transverse momentum while they are at most of the order of +3% above $p_T \approx 250$ GeV. As in the previous case, the uncertainties due to missing higher-order corrections dominate over those due to matching for most of the plotted spectrum. For the POWHEG BOX prediction, the scale uncertainties start out very symmetric with ±20% but grow more and more asymmetric toward the end of the plotted range with estimated uncertainties of +5% and −20%. A similar trend is not visible for MG5_aMC@NLO predictions, as uncertainties are slightly asymmetric from the start with −25% and +16% for small transverse momenta and −30% and +12% uncertainties in the tail of the distribution. For the POWHEG BOX matching uncertainties never exceed ±3%, while for MG5_aMC@NLO they become as large as 10% in the tail of the distribution.

Next we discuss the invariant mass distribution of the four top quarks shown in the left panel of Fig. 3. We observe that the EW contributions are sizable not only at the production threshold $M_{t\bar{t}t\bar{t}} \sim 4m_t$ but also in the high-energy tail of the distribution. To be specific, we find sizable corrections of the order of +20% in the threshold region that then decrease down to +5% at intermediate value of the invariant mass of around 1.2 TeV. However, the leading order EW production channels give rise to +10% corrections in the

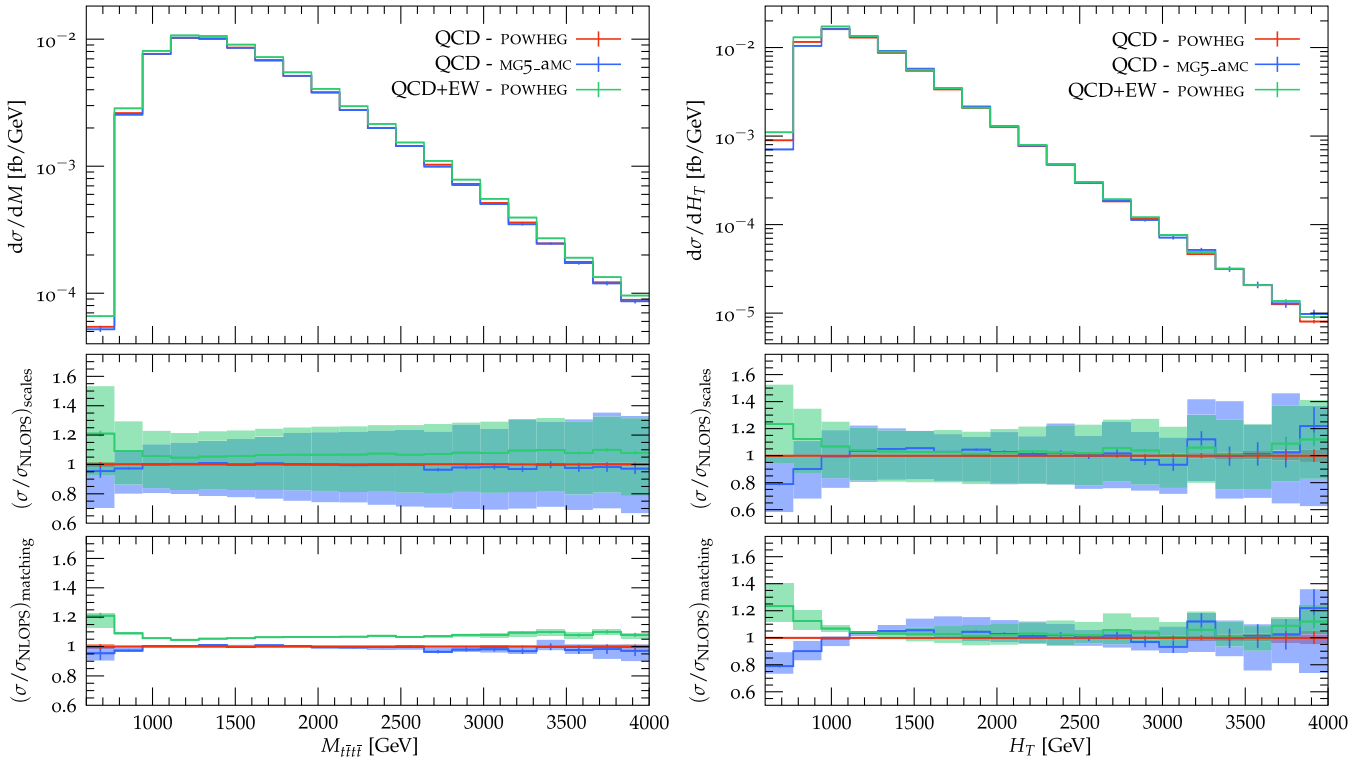

FIG. 3. Differential cross section distribution as a function of the invariant mass of the four top quarks (left) and of the H_T observable (right) for the $pp \to t\bar{t}t\bar{t}$ process. The uncertainty bands correspond to independent variations of the renormalization and factorization scales (middle panel) and of the matching parameters (bottom panel).

very high-energetic tail of the distribution. The matching uncertainties are for all theoretical predictions small and estimated to be below 5%, where in the case of POWHEG BOX they are the smallest. However, the uncertainties originating from the choice of renormalization and factorization scales are between 20%–30% over the whole spectrum.

We now turn to the H_T distribution, as defined in Eq. (6), depicted in the right panel of Fig. 3. Independently of the employed matching scheme and the inclusion of EW contributions, we find excellent agreement between all predictions above $H_T \approx 1.2$ TeV with differences below 3%. Only in the first three bins we encounter sizable differences between the various approaches. For instance, the MG5_aMC@NLO prediction is up to 20% smaller at the beginning of spectrum if compared to the corresponding POWHEG BOX prediction that takes into account the same perturbative corrections. We observe that EW contributions are sizable here as well and yield a +23% enhancement in the low tail. Matching uncertainties are larger than in the previous observables and reach up to ±10% in the case of POWHEG BOX, and up to ±25% in the case of MG5_aMC@NLO. On the other hand, scale uncertainties are at most ±25% for POWHEG BOX predictions and in the case of MG5_aMC@NLO they reach ±30%.

Finally, we discuss the transverse momentum and the pseudorapidity distribution of the leading jet as shown in Fig. 4. Contrary to all previous observables, these two distributions are only predicted at leading order accuracy. Nonetheless, they are useful for exploring differences between the POWHEG and the MC@NLO matching schemes. Let us start with the transverse momentum distribution. Here we find large differences between MG5_aMC@NLO and POWHEG BOX up to 35% at transverse momenta of the order of 150 GeV. Furthermore, MG5_aMC@NLO predicts a softer spectrum in the tail of the distribution. The corresponding theoretical uncertainties are large as well and their bands include predictions from the other event generators, respectively, throughout the majority of the spectrum. In all cases scale uncertainties start around ±25% and grow up to ±55% at the end of the plotted range. In addition, the spectrum exhibits a sizable dependence on the parton-shower matching related parameters. In the case of POWHEG BOX matching uncertainties are estimated to be of the order of ±6% at the beginning and increase up to ±25% at the end of the distribution. On the other hand, for MG5_aMC@NLO the initial shower scale dependence is rather different, while the beginning and end of the spectrum have modest uncertainties of the order of ±10% they grow as large as 95% in the intermediate range. Thus, the choice of initial shower scale μ_Q has a severe impact on the shape of the distribution.

At last, let us turn to the pseudorapidity distribution as depicted on the right of Fig. 4. Also for this observable, we find sizable difference between the various predictions.

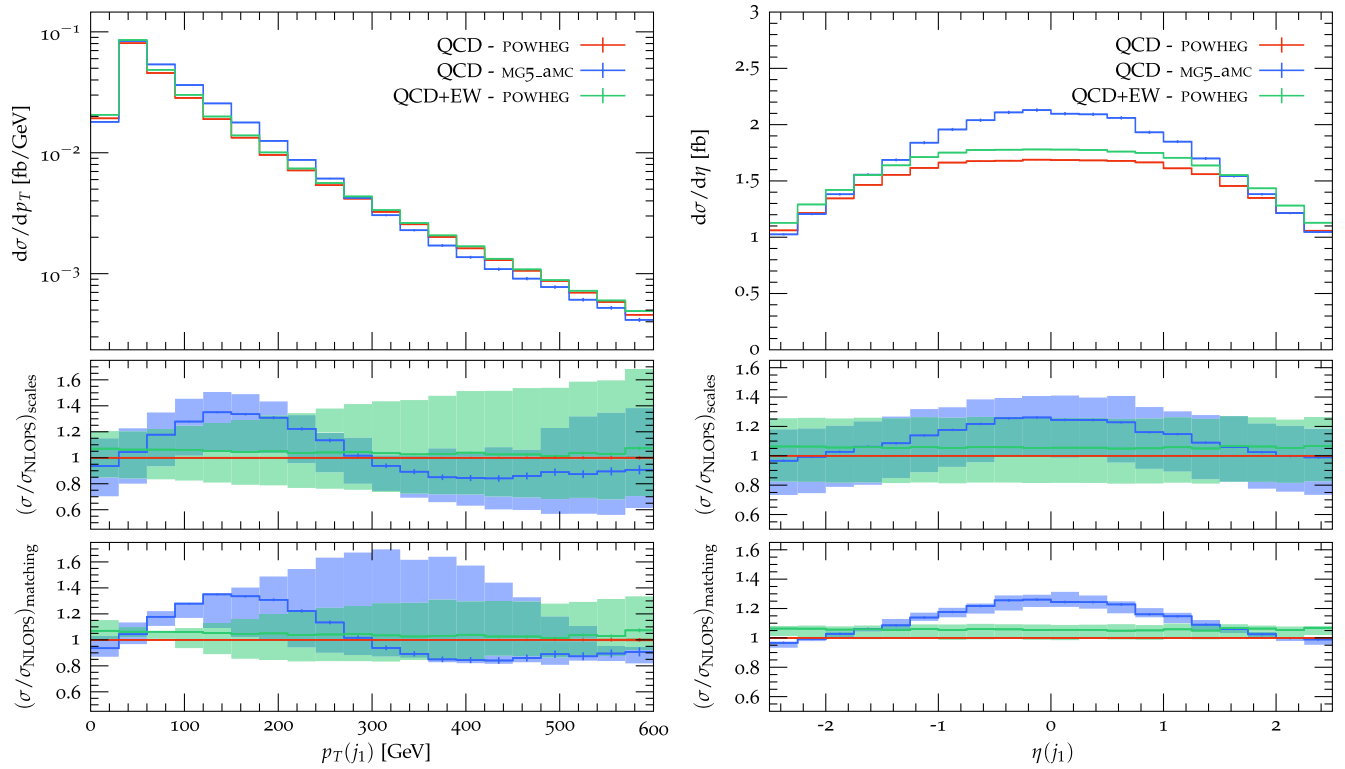

FIG. 4. Differential cross section distribution as a function of the transverse momentum (left) and of the pseudorapidity (right) of the hardest jet for the $pp \to t\bar{t}t\bar{t}$ process. The uncertainty bands correspond to independent variations of the renormalization and factorization scales (middle panel) and of the matching parameters (bottom panel).

The impact of the EW production modes is modest and yields rather constant positive corrections at the level of 5%–7% over the whole spectrum. The largest differences are found when different matching schemes are employed. The MG5_aMC@NLO predictions is considerably larger by nearly 25% in the central rapidity region as compared to the POWHEG BOX prediction that also includes only pure QCD corrections. In all cases, the scale uncertainty is the dominant contribution to the theoretical uncertainty and amounts to a constant $\pm 20\%$ over whole plotted range.

Similar differences in the modeling of the leading jet between MG5_aMC@NLO and the POWHEG BOX have been already observed for the $pp \to t\bar{t}b\bar{b}$ and $pp \to t\bar{t}W^{\pm}$ processes, as discussed in Refs. [68,80,92,93].

C. Single lepton plus jets signature

In the following we study a single lepton plus jets signature in order to investigate the impact of spin-correlated top-quark decays and the impact of the leading order EW contributions at the fiducial level. The signature is characterized by the presence of exactly one charged lepton ℓ, with $\ell = e, \mu$, at least $4b$ jets and at least 6 light jets. The lepton has to fulfill $p_T(\ell) > 15$ GeV and $|y(\ell)| < 2.5$. Jets are formed using the anti-k_T jet algorithm with $R = 0.4$ and a jet is labeled a b jet if at least one of its constituents is a heavy b quark. Light as well as b jets have to pass the $p_T(j) > 25$ GeV and $|y(j)| < 2.5$ cuts. The definition of the fiducial phase space volume is inspired by Ref. [17].

We show in the following only theoretical predictions obtained with our POWHEG BOX implementation. We consider three predictions: one prediction that includes both spin correlations in the decay of the top quark as well as the subleading EW channels, and two predictions with either the first or the second improvement switched off. If spin correlations are omitted the decays of top quarks and W bosons are generated via independent $1 \to 2$ decays. We do not discuss matching uncertainties here anymore as we have seen in the previous section that theoretical uncertainties are dominated by missing higher-order corrections. Moreover, matching uncertainties are expected to be very similar between the various predictions as they are all based on POWHEG BOX.

For the integrated fiducial cross section we obtain for the three approaches the following results:

$$\begin{aligned}
\sigma^{\text{spin}}_{\text{QCD}} &= 0.618^{+0.119\ (19\%)}_{-0.142\ (23\%)}\ \text{fb}, \\
\sigma^{\text{spin}}_{\text{QCD+EW}} &= 0.649^{+0.117\ (18\%)}_{-0.144\ (22\%)}\ \text{fb}, \\
\sigma^{\text{no-spin}}_{\text{QCD+EW}} &= 0.625^{+0.114\ (18\%)}_{-0.139\ (22\%)}\ \text{fb}.
\end{aligned} \tag{12}$$

We observe that EW contributions and spin-correlated decays have opposite effects on the fiducial cross section.

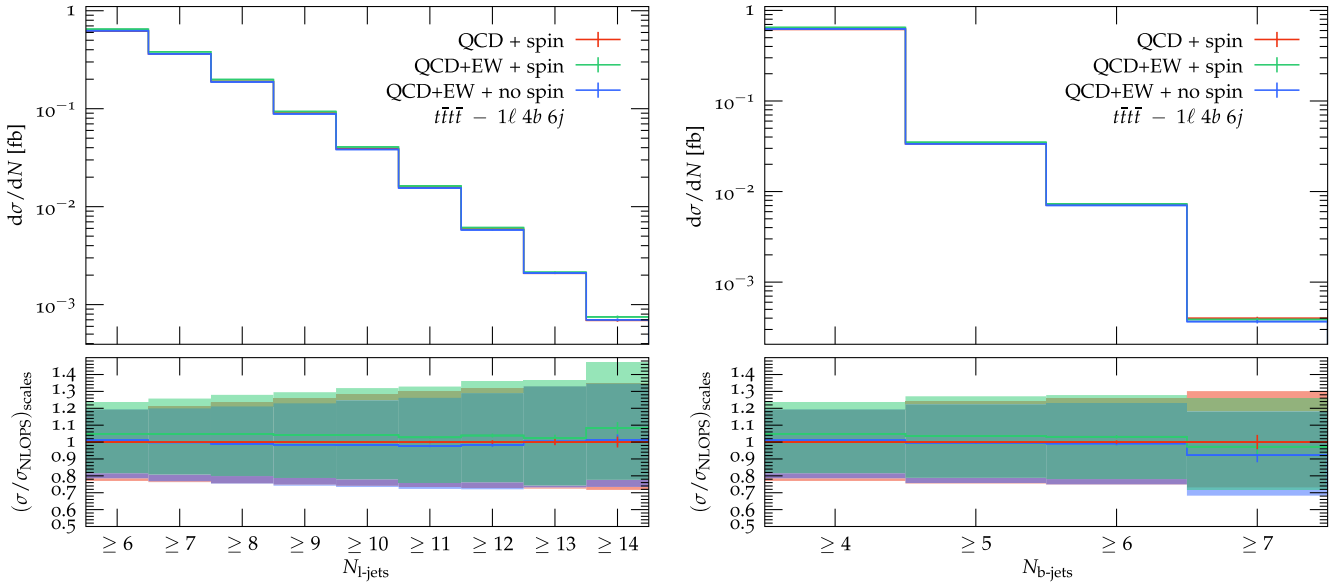

FIG. 5. Inclusive cross sections in the single lepton fiducial region as a function of the number of light jets (left) and the number of b jets (right) for the $pp \to t\bar{t}t\bar{t}$ process. The uncertainty bands correspond to independent variations of the renormalization and factorization scales (bottom panel).

For spin-correlated decays the electroweak production modes increase the cross section by 5% with respect to the QCD only predictions. On the other hand, if spin correlations are ignored then cross sections decreases by 4%. Even though all predictions for integrated cross sections are compatible within the scale uncertainty of roughly ±20%, we will see in the following that this is not necessarily the case at the differential level.

We next inspect the inclusive cross section as a function of the number of light and b jets as shown in Fig. 5. For both observables we recognize essentially the same pattern, independently of the number of jets, with respect to spin correlations and EW production modes as discussed before. However, theoretical uncertainties grow with increasing number of jets. For instance, uncertainties for the cross section as a function of the number of light jets are of the order of ±22% for at least 6 jets and they increase up to ±36% for events with at least 14 jets. Furthermore, nearly 15% of all $pp \to t\bar{t}t\bar{t}$ events are accompanied by at least 9 light jets and only 1% of all events in this signature are associated with at least 12 light jets. On the contrary, the corresponding distribution as a function of the number of b jets falls off more steeply. This is expected, as the dominant source of additional b jets, besides the $4b$ jets originating from the top-quark decays, are $g \to b\bar{b}$ splittings in the parton-shower evolution. Additionally, initial state $b \to gb$ splittings occur as part of the real radiation contribution of the NLO QCD corrections as well as during the parton shower evolution. Nonetheless, these contributions are heavily suppressed by the b-quark parton distribution function. For instance, only 5% of all events have one additional b jet. The theoretical uncertainties as estimated from independent scale variations start again from ±22% and increase up to ±30% for at least $7b$ jets. Note that for more realistic estimates of perturbative uncertainties of both cross sections as function of light and b jets in bins beyond the first one shower scale variations should be considered.

Next we discuss hadronic observables such as the transverse momentum of the hardest b jet as shown in the left panel of Fig. 6. First of all we notice that the spectrum is extremely hard. Between the peak of the distribution for transverse momenta around 150 GeV and the tail at 1 TeV the cross section does not drop even 3 orders of magnitude. Similar features have been observed for the $pp \to t\bar{t}b\bar{b}$ process in Refs. [94,95] for final states with 4 b jets. The scale uncertainties are rather constant over the whole plotted range and are estimated to be between ±25% and ±20%, where the tail of the distribution exhibits smaller uncertainties. Furthermore, we find a significant contribution of up to +10% due to the inclusion of the EW production channels for transverse momenta below 200 GeV.

We now turn to the H_T observable as depicted on the right of Fig. 6. At the fiducial level we define H_T via

$$H_T = p_T(\ell) + p_T^{\text{miss}} + \sum_{i=10}^{N_{\text{jets}}} p_T(j_i), \tag{13}$$

where we do not distinguish between light and b jets. For this observable we find an even larger impact due to the leading order EW production channels of up to +25% below 1 TeV. Above, they only contribute a rather constant +3% amount for the rest of the plotted range. Spin correlation effects have also only a mild impact on the tail

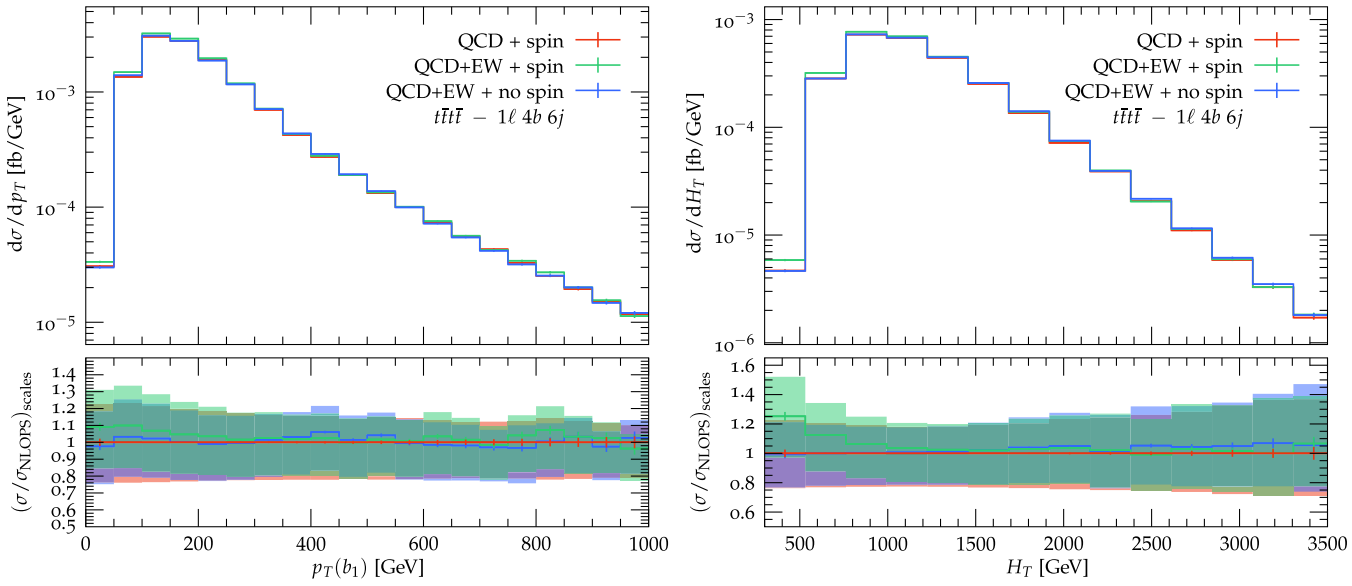

FIG. 6. Differential cross section distribution in the single lepton fiducial region as a function of the transverse momentum of the hardest b jet (left) and of the H_T observable (right) for the $pp \to t\bar{t}t\bar{t}$ process. The uncertainty bands correspond to independent variations of the renormalization and factorization scales (bottom panel).

of the distribution. They soften the spectrum by roughly 5%. Scale uncertainties are estimated to be $\pm 22\%$ at the beginning of the spectrum which then increases up to $\pm 35\%$ at the end of the plotted range.

Now we discuss two angular observables that are used for the discrimination of the signal from the background in the experimental analysis of Ref. [17]. To this end, we show in Fig. 7 the minimal distance ΔR among all pairs of b jets, $\Delta R_{bb}^{\min}$, as well as among all b jets and the lepton, $\Delta R_{b\ell}^{\min}$. For both angular distributions we find strong enhancements in the tails of the distributions due to the EW production of the $pp \to t\bar{t}t\bar{t}$ process. To be specific, we find corrections up to $+27\%$ for $\Delta R_{bb}^{\min}$ and up to $+11\%$ for $\Delta R_{b\ell}^{\min}$. The scale uncertainties are below $\pm 26\%$ in the whole plotted range and spin correlations only have a very mild impact that lead to minor shape differences.

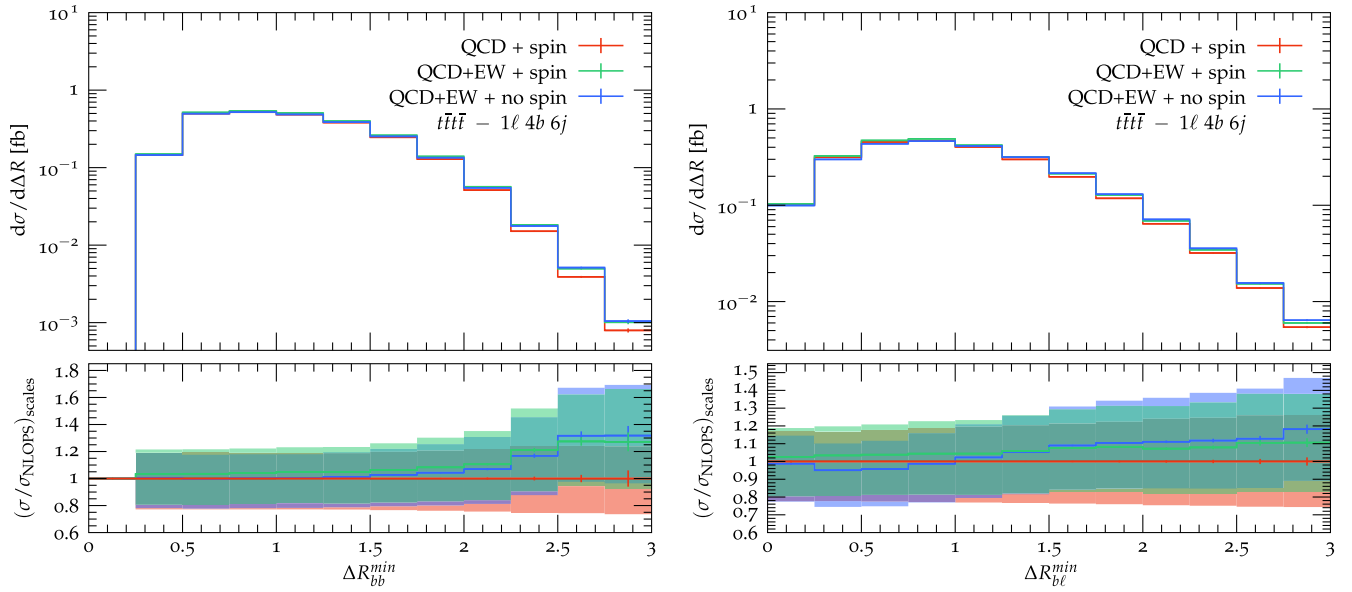

FIG. 7. Differential cross section distribution in the single lepton fiducial region as a function of the minimal ΔR between all b jet pairs (left) and of the minimal ΔR between all b jets and the lepton (right) for the $pp \to t\bar{t}t\bar{t}$ process. The uncertainty bands correspond to independent variations of the renormalization and factorization scales (bottom panel).

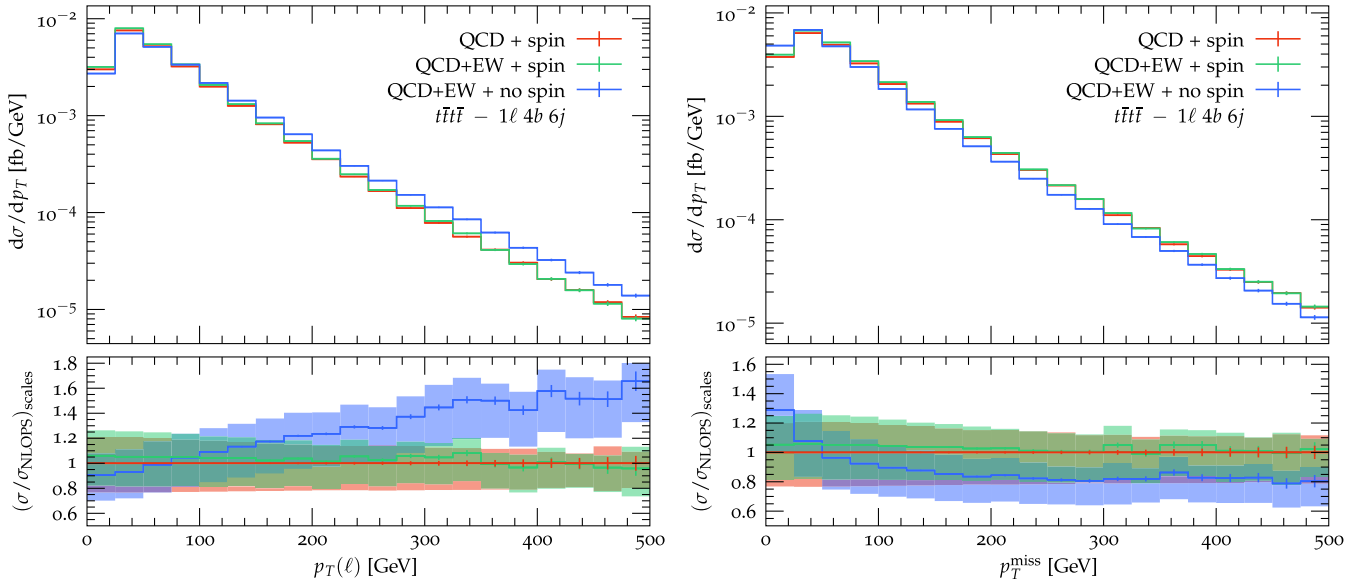

FIG. 8. Differential cross section distribution in the single lepton fiducial region as a function of the transverse momentum of the lepton (left) and of the missing transverse momentum (right) for the $pp \to t\bar{t}t\bar{t}$ process. The uncertainty bands correspond to independent variations of the renormalization and factorization scales (bottom panel).

At last we turn to leptonic observables. We show the transverse momentum of the charged lepton on the left and the missing transverse momentum in the right panel of Fig. 8. For both observable we notice that spin correlations have to be taken into as they have a tremendous impact on the shape of the differential distribution. The transverse momentum distribution of the charged lepton is much harder if correlations are omitted and overshoots the tail of the distribution by nearly 60%. These deviations are not covered by the estimated theoretical uncertainties which are of the order of 20%–25% over the whole plotted range.

Also for the missing transverse momentum we find large shape differences. However, in this case the distribution becomes softer as compared to the case when spin-correlated top-quark decays are taken into account. While there are significantly more events with low values of p_T^{miss} if uncorrelated decays are considered, for $p_T^{\text{miss}} \gtrsim 250$ GeV the spectrum is nearly constant -20% smaller than predictions that take spin correlations into account. Furthermore, the scale uncertainties are independent of the treatment of decays and EW production modes of the order of $\pm 20\%$.

V. CONCLUSIONS

In this article we presented an implementation of the production of four top quarks at hadron colliders in the POWHEG BOX framework. Besides taking into account the leading NLO QCD corrections at $\mathcal{O}(\alpha_s^5)$ we also include formally subleading EW production channels at LO accuracy. Furthermore, our implementation allows to decay top quarks at LO accuracy retaining spin-correlation effects. This feature made it possible to study the effects of spin-correlations in top-quark decays in this process for the first time.

We first investigated the impact of leading NLO QCD corrections and subleading EW channels on the total cross sections. We find that QCD corrections contribute at up to slightly over $+50\%$ and EW modes at the $+5\%$ to $+10\%$ level. The inclusion of leading NLO corrections leads to a reduction of scale uncertainties from up to 70% down to at most 22%. Thus the inclusion of NLO QCD corrections as well as the subleading EW channels is essential for reliable predictions of four top production.

We investigated modeling differences for the inclusive $pp \to t\bar{t}t\bar{t}$ production process with stable top-quarks at the 13 TeV LHC by comparing MG5_aMC@NLO and POWHEG BOX. We find very good overall agreement between the two frameworks for observables at NLO accuracy, with only minor differences due to the shower evolution in the threshold region. We do also find notable deviations in the hardest light jet spectra, predicted at LO accuracy, which coincides with findings in other production modes of associated top pair production. We also investigated the impact of the EW production channels at the differential level and estimated matching as well as scale uncertainties. We observe that the impact of these subleading channels is generally below 10% but can exceed that near the production threshold. Nonetheless, their inclusion represents a systematic improvement over pure NLO QCD predictions.

Furthermore, we also investigated a single lepton plus jets signature as it is currently employed for $pp \to t\bar{t}t\bar{t}$ cross section measurements and addressed for the first time the size of the subleading EW contributions at the fiducial level.

In this case they can reach up to nearly 40% in distributions used for signal/background discriminants in experimental analyses. We also studied the impact of spin-correlated top-quark decays and found that they are essential to obtain a reliable description of leptonic observables. We want to stress that spin-correlation effects are indispensable also for multi-lepton signatures as their impact is a general feature for leptonic observables and signature independent. Finally, we also estimated theoretical uncertainties due to missing higher-order corrections.

The $pp \to t\bar{t}t\bar{t}$ process still awaits its full discovery at the LHC. Once, it is observed it will be instrumental in constraining possible new physics. We are hopeful, that this new tool will help to study more accurately the SM dynamics of the four top quark production process.

ACKNOWLEDGMENTS

The authors want to thank Silvia Ferrario Ravasio and Laura Reina for comments on the manuscript. The work of T. J. was supported by the DFG under Grant No. 396021762—TRR 257 and through Project-ID No. 273811115—SFB 1225 "ISOQUANT", and the Research Training Network 2149 "Strong and weak interactions—from hadrons to dark matter". M. K. thanks Fernando Febres Cordero and Laura Reina for helpful discussions. The work of M. K. is supported in part by the U.S. Department of Energy under Grant No. DE-SC0010102. The computing for this project was performed on the HPC cluster at the Research Computing Center at the Florida State University (FSU).

[1] F. Abe *et al.* (CDF Collaboration), Evidence for top quark production in $\bar{p}p$ collisions at $\sqrt{s} = 1.8$ TeV, Phys. Rev. D **50**, 2966 (1994).
[2] F. Abe *et al.* (CDF Collaboration), Observation of Top Quark Production in $\bar{p}p$ Collisions, Phys. Rev. Lett. **74**, 2626 (1995).
[3] S. Abachi *et al.* (D0 Collaboration), Observation of the Top Quark, Phys. Rev. Lett. **74**, 2632 (1995).
[4] Georges Aad *et al.* (ATLAS Collaboration), Observation of top-quark pair production in association with a photon and measurement of the $t\bar{t}\gamma$ production cross section in pp collisions at $\sqrt{s} = 7$ TeV using the ATLAS detector, Phys. Rev. D **91**, 072007 (2015).
[5] Albert M. Sirunyan *et al.* (CMS Collaboration), Measurement of the semileptonic $\mathrm{t\bar{t}} + \gamma$ production cross section in pp collisions at $\sqrt{s} = 8$ TeV, J. High Energy Phys. 10 (2017) 006.
[6] Albert M. Sirunyan *et al.* (CMS Collaboration), Measurement of the cross section for top quark pair production in association with a W or Z boson in proton-proton collisions at $\sqrt{s} = 13$ TeV, J. High Energy Phys. 08 (2018) 011.
[7] Morad Aaboud *et al.* (ATLAS Collaboration), Measurement of the $t\bar{t}Z$ and $t\bar{t}W$ cross sections in proton-proton collisions at $\sqrt{s} = 13$ TeV with the ATLAS detector, Phys. Rev. D **99**, 072009 (2019).
[8] Albert M. Sirunyan *et al.* (CMS Collaboration), Observation of $t\bar{t}H$ Production, Phys. Rev. Lett. **120**, 231801 (2018).
[9] M. Aaboud *et al.* (ATLAS Collaboration), Observation of Higgs boson production in association with a top quark pair at the LHC with the ATLAS detector, Phys. Lett. B **784**, 173 (2018).
[10] Morad Aaboud *et al.* (ATLAS Collaboration), Search for four-top-quark production in the single-lepton and opposite-sign dilepton final states in pp collisions at $\sqrt{s} = 13$ TeV with the ATLAS detector, Phys. Rev. D **99**, 052009 (2019).
[11] Georges Aad *et al.* (ATLAS Collaboration), Evidence for $t\bar{t}t\bar{t}$ production in the multilepton final state in proton–proton collisions at $\sqrt{s} = 13$ TeV with the ATLAS detector, Eur. Phys. J. C **80**, 1085 (2020).
[12] Vardan Khachatryan *et al.* (CMS Collaboration), Search for standard model production of four top quarks in the lepton + jets channel in pp collisions at $\sqrt{s} = 8$ TeV, J. High Energy Phys. 11 (2014) 154.
[13] A. M. Sirunyan *et al.* (CMS Collaboration), Search for standard model production of four top quarks in proton-proton collisions at $\sqrt{s} = 13$ TeV, Phys. Lett. B **772**, 336 (2017).
[14] Albert M. Sirunyan *et al.* (CMS Collaboration), Search for standard model production of four top quarks with same-sign and multilepton final states in proton–proton collisions at $\sqrt{s} = 13$ TeV, Eur. Phys. J. C **78**, 140 (2018).
[15] Albert M. Sirunyan *et al.* (CMS Collaboration), Search for the production of four top quarks in the single-lepton and opposite-sign dilepton final states in proton-proton collisions at $\sqrt{s} = 13$ TeV, J. High Energy Phys. 11 (2019) 082.
[16] Albert M. Sirunyan *et al.* (CMS Collaboration), Search for production of four top quarks in final states with same-sign or multiple leptons in proton-proton collisions at $\sqrt{s} = 13$ TeV, Eur. Phys. J. C **80**, 75 (2020).
[17] Georges Aad *et al.* (ATLAS Collaboration), Measurement of the $t\bar{t}t\bar{t}$ production cross section in pp collisions at $\sqrt{s} =$ 13 TeV with the ATLAS detector, J. High Energy Phys. 11 (2021) 118.
[18] Ben Lillie, Jing Shu, and Timothy M. P. Tait, Top compositeness at the Tevatron and LHC, J. High Energy Phys. 04 (2008) 087.
[19] Kunal Kumar, Tim M. P. Tait, and Roberto Vega-Morales, Manifestations of top compositeness at colliders, J. High Energy Phys. 05 (2009) 022.
[20] Giacomo Cacciapaglia, Roberto Chierici, Aldo Deandrea, Luca Panizzi, Stephane Perries, and Silvano Tosi, Four tops on the real projective plane at LHC, J. High Energy Phys. 10 (2011) 042.

[21] Maxim Perelstein and Andrew Spray, Four boosted tops from a Regge gluon, J. High Energy Phys. 09 (2011) 008.
[22] J. A. Aguilar-Saavedra and Jose Santiago, Four tops and the $t\bar{t}$ forward-backward asymmetry, Phys. Rev. D **85**, 034021 (2012).
[23] Lana Beck, Freya Blekman, Didar Dobur, Benjamin Fuks, James Keaveney, and Kentarou Mawatari, Probing top-philic sgluons with LHC Run I data, Phys. Lett. B **746**, 48 (2015).
[24] Ezequiel Alvarez, Darius A. Faroughy, Jernej F. Kamenik, Roberto Morales, and Alejandro Szynkman, Four tops for LHC, Nucl. Phys. **B915**, 19 (2017).
[25] Ezequiel Alvarez, Aurelio Juste, and Rosa María Sandá Seoane, Four-top as probe of light top-philic new physics, J. High Energy Phys. 12 (2019) 080.
[26] Ezequiel Alvarez, Barry M. Dillon, Darius A. Faroughy, Jernej F. Kamenik, Federico Lamagna, and Manuel Szewc, Bayesian probabilistic modeling for four-top production at the LHC, Phys. Rev. D **105**, 092001 (2022).
[27] Linda M. Carpenter, Taylor Murphy, and Matthew J. Smylie, $t\bar{t}t\bar{t}$ signatures through the lens of color-octet scalars, J. High Energy Phys. 01 (2022) 047.
[28] Hans Peter Nilles, Supersymmetry, supergravity and particle physics, Phys. Rep. **110**, 1 (1984).
[29] Glennys R. Farrar and Pierre Fayet, Phenomenology of the production, decay, and detection of new hadronic states associated with supersymmetry, Phys. Lett. **76B**, 575 (1978).
[30] Manuel Toharia and James D. Wells, Gluino decays with heavier scalar superpartners, J. High Energy Phys. 02 (2006) 015.
[31] Daniele Alves (LHC New Physics Working Group), Simplified models for LHC new physics searches, J. Phys. G **39**, 105005 (2012).
[32] D. Dicus, A. Stange, and S. Willenbrock, Higgs decay to top quarks at hadron colliders, Phys. Lett. B **333**, 126 (1994).
[33] Nathaniel Craig, Francesco D'Eramo, Patrick Draper, Scott Thomas, and Hao Zhang, The hunt for the rest of the Higgs bosons, J. High Energy Phys. 06 (2015) 137.
[34] Nathaniel Craig, Jan Hajer, Ying-Ying Li, Tao Liu, and Hao Zhang, Heavy Higgs bosons at low tan β: From the LHC to 100 TeV, J. High Energy Phys. 01 (2017) 018.
[35] Giorgio Busoni *et al.*, Recommendations on presenting LHC searches for missing transverse energy signals using simplified *s*-channel models of dark matter, Phys. Dark Universe **27**, 100365 (2020).
[36] Andreas Albert *et al.*, Recommendations of the LHC dark matter working group: Comparing LHC searches for dark matter mediators in visible and invisible decay channels and calculations of the thermal relic density, Phys. Dark Universe **26**, 100377 (2019).
[37] G. F. Giudice, C. Grojean, A. Pomarol, and R. Rattazzi, The strongly-interacting light Higgs, J. High Energy Phys. 06 (2007) 045.
[38] Alex Pomarol and Javi Serra, Top quark compositeness: Feasibility and implications, Phys. Rev. D **78**, 074026 (2008).
[39] Giovanni Banelli, Ennio Salvioni, Javi Serra, Tobias Theil, and Andreas Weiler, The present and future of four top operators, J. High Energy Phys. 02 (2021) 043.
[40] Cen Zhang, Constraining *qqtt* operators from four-top production: A case for enhanced EFT sensitivity, Chin. Phys. C **42**, 023104 (2018).
[41] D. Barducci *et al.*, Interpreting top-quark LHC measurements in the standard-model effective field theory, arXiv:1802.07237.
[42] Nathan P. Hartland, Fabio Maltoni, Emanuele R. Nocera, Juan Rojo, Emma Slade, Eleni Vryonidou, and Cen Zhang, A Monte Carlo global analysis of the standard model effective field theory: The top quark sector, J. High Energy Phys. 04 (2019) 100.
[43] Jacob J. Ethier, Giacomo Magni, Fabio Maltoni, Luca Mantani, Emanuele R. Nocera, Juan Rojo, Emma Slade, Eleni Vryonidou, and Cen Zhang (SMEFiT Collaboration), Combined SMEFT interpretation of Higgs, diboson, and top quark data from the LHC, J. High Energy Phys. 11 (2021) 089.
[44] Luc Darmé, Benjamin Fuks, and Mark Goodsell, Cornering sgluons with four-top-quark events, Phys. Lett. B **784**, 223 (2018).
[45] Qing-Hong Cao, Jun-Ning Fu, Yandong Liu, Xiao-Hu Wang, and Rui Zhang, Probing top-philic new physics via four-top-quark production, Chin. Phys. C **45**, 093107 (2021).
[46] Luc Darmé, Benjamin Fuks, and Fabio Maltoni, Top-philic heavy resonances in four-top final states and their EFT interpretation, J. High Energy Phys. 09 (2021) 143.
[47] Qing-Hong Cao, Shao-Long Chen, and Yandong Liu, Probing Higgs width and top quark Yukawa coupling from $t\bar{t}H$ and $t\bar{t}t\bar{t}$ productions, Phys. Rev. D **95**, 053004 (2017).
[48] Qing-Hong Cao, Shao-Long Chen, Yandong Liu, Rui Zhang, and Ya Zhang, Limiting top quark-Higgs boson interaction and Higgs-boson width from multitop productions, Phys. Rev. D **99**, 113003 (2019).
[49] G. Bevilacqua and M. Worek, Constraining BSM physics at the LHC: Four top final states with NLO accuracy in perturbative QCD, J. High Energy Phys. 07 (2012) 111.
[50] Fabio Maltoni, Davide Pagani, and Ioannis Tsinikos, Associated production of a top-quark pair with vector bosons at NLO in QCD: Impact on $t\bar{t}H$ searches at the LHC, J. High Energy Phys. 02 (2016) 113.
[51] Rikkert Frederix, Davide Pagani, and Marco Zaro, Large NLO corrections in $t\bar{t}W^{\pm}$ and $t\bar{t}t\bar{t}$ hadroproduction from supposedly subleading EW contributions, J. High Energy Phys. 02 (2018) 031.
[52] Stefano Frixione and Bryan R. Webber, Matching NLO QCD computations and parton shower simulations, J. High Energy Phys. 06 (2002) 029.
[53] Stefano Frixione, Paolo Nason, and Bryan R. Webber, Matching NLO QCD and parton showers in heavy flavor production, J. High Energy Phys. 08 (2003) 007.
[54] J. Alwall, R. Frederix, S. Frixione, V. Hirschi, F. Maltoni, O. Mattelaer, H. S. Shao, T. Stelzer, P. Torrielli, and M. Zaro, The automated computation of tree-level and next-to-leading order differential cross sections, and their matching to parton shower simulations, J. High Energy Phys. 07 (2014) 079.
[55] R. Frederix, S. Frixione, V. Hirschi, D. Pagani, H. S. Shao, and M. Zaro, The automation of next-to-leading order

electroweak calculations, J. High Energy Phys. 07 (2018) 185.
[56] T. Gleisberg, S. Hoeche, F. Krauss, M. Schonherr, S. Schumann, F. Siegert, and J. Winter, Event generation with SHERPA1.1, J. High Energy Phys. 02 (2009) 007.
[57] Enrico Bothmann *et al.* (Sherpa Collaboration), Event generation with SHERPA2.2, SciPost Phys. **7**, 034 (2019).
[58] ATLAS Collaboration, Modelling of rare top quark processes at $\sqrt{s} = 13$ TeV in ATLAS, Report No. ATL-PHYS-PUB-2020-024, 2020.
[59] Paolo Nason, A new method for combining NLO QCD with shower Monte Carlo algorithms, J. High Energy Phys. 11 (2004) 040.
[60] Simone Alioli, Paolo Nason, Carlo Oleari, and Emanuele Re, A general framework for implementing NLO calculations in shower Monte Carlo programs: The POWHEG BOX, J. High Energy Phys. 06 (2010) 043.
[61] J. H. Kühn, A. Scharf, and P. Uwer, Weak interactions in top-quark pair production at hadron colliders: An update, Phys. Rev. D **91**, 014020 (2015).
[62] Martin Beneke, Andreas Maier, Jan Piclum, and Thomas Rauh, Higgs effects in top anti-top production near threshold in e^+e^- annihilation, Nucl. Phys. **B899**, 180 (2015).
[63] Fabio Cascioli, Philipp Maierhofer, and Stefano Pozzorini, Scattering Amplitudes with Open Loops, Phys. Rev. Lett. **108**, 111601 (2012).
[64] Federico Buccioni, Stefano Pozzorini, and Max Zoller, On-the-fly reduction of open loops, Eur. Phys. J. C **78**, 70 (2018).
[65] Federico Buccioni, Jean-Nicolas Lang, Jonas M. Lindert, Philipp Maierhöfer, Stefano Pozzorini, Hantian Zhang, and Max F. Zoller, OpenLoops 2, Eur. Phys. J. C **79**, 866 (2019).
[66] Tomáš Ježo, Jonas M. Lindert, Paolo Nason, Carlo Oleari, and Stefano Pozzorini, An NLO + PS generator for $t\bar{t}$ and Wt production and decay including nonresonant and interference effects, Eur. Phys. J. C **76**, 691 (2016).
[67] Stefano Frixione, Eric Laenen, Patrick Motylinski, and Bryan R. Webber, Angular correlations of lepton pairs from vector boson and top quark decays in Monte Carlo simulations, J. High Energy Phys. 04 (2007) 081.
[68] F. Febres Cordero, M. Kraus, and L. Reina, Top-quark pair production in association with a $W^{\pm}$ gauge boson in the POWHEG-BOX, Phys. Rev. D **103**, 094014 (2021).
[69] Aggeliki Kanaki and Costas G. Papadopoulos, HELAC: A package to compute electroweak helicity amplitudes, Comput. Phys. Commun. **132**, 306 (2000).
[70] Costas G. Papadopoulos, PHEGAS: A phase space generator for automatic cross-section computation, Comput. Phys. Commun. **137**, 247 (2001).
[71] Alessandro Cafarella, Costas G. Papadopoulos, and Malgorzata Worek, Helac-Phegas: A generator for all parton level processes, Comput. Phys. Commun. **180**, 1941 (2009).
[72] Pierre Artoisenet, Rikkert Frederix, Olivier Mattelaer, and Robbert Rietkerk, Automatic spin-entangled decays of heavy resonances in Monte Carlo simulations, J. High Energy Phys. 03 (2013) 015.
[73] Ansgar Denner, S. Dittmaier, M. Roth, and D. Wackeroth, Electroweak radiative corrections to $e + e \to \mathrm{W}\,\mathrm{W} \to 4$ fermions in double pole approximation: The RACOONWW approach, Nucl. Phys. **B587**, 67 (2000).
[74] John M. Campbell and R. Keith Ellis, Top-quark processes at NLO in production and decay, J. Phys. G **42**, 015005 (2015).
[75] Richard D. Ball *et al.* (NNPDF Collaboration), Parton distributions from high-precision collider data, Eur. Phys. J. C **77**, 663 (2017).
[76] Andy Buckley, James Ferrando, Stephen Lloyd, Karl Nordström, Ben Page, Martin Rüfenacht, Marek Schönherr, and Graeme Watt, LHAPDF6: Parton density access in the LHC precision era, Eur. Phys. J. C **75**, 132 (2015).
[77] Simone Alioli, Paolo Nason, Carlo Oleari, and Emanuele Re, NLO vector-boson production matched with shower in POWHEG, J. High Energy Phys. 07 (2008) 060.
[78] Simone Alioli, Paolo Nason, Carlo Oleari, and Emanuele Re, NLO Higgs boson production via gluon fusion matched with shower in POWHEG, J. High Energy Phys. 04 (2009) 002.
[79] Tomáš Ježo, Jonas M. Lindert, Niccolo Moretti, and Stefano Pozzorini, New NLOPS predictions for $t\bar{t} + b$ -jet production at the LHC, Eur. Phys. J. C **78**, 502 (2018).
[80] G. Bevilacqua, H. Y. Bi, F. Febres Cordero, H. B. Hartanto, M. Kraus, J. Nasufi, L. Reina, and M. Worek, Modeling uncertainties of $t\bar{t}W^{\pm}$ multilepton signatures, Phys. Rev. D **105**, 014018 (2022).
[81] Torbjorn Sjostrand, Stephen Mrenna, and Peter Z. Skands, PYTHIA6.4 physics and manual, J. High Energy Phys. 05 (2006) 026.
[82] Torbjörn Sjöstrand, Stefan Ask, Jesper R. Christiansen, Richard Corke, Nishita Desai, Philip Ilten, Stephen Mrenna, Stefan Prestel, Christine O. Rasmussen, and Peter Z. Skands, An introduction to PYTHIA8.2, Comput. Phys. Commun. **191**, 159 (2015).
[83] Andy Buckley, Jonathan Butterworth, David Grellscheid, Hendrik Hoeth, Leif Lonnblad, James Monk, Holger Schulz, and Frank Siegert, RIVET user manual, Comput. Phys. Commun. **184**, 2803 (2013).
[84] Christian Bierlich *et al.*, Robust independent validation of experiment and theory: RIVET version 3, SciPost Phys. **8**, 026 (2020).
[85] See Supplemental Material at http://link.aps.org/supplemental/10.1103/PhysRevD.105.114024 for the numerical data of all shown observables, the Rivet analysis files as well as parton shower input settings.
[86] L. A. Harland-Lang, A. D. Martin, P. Motylinski, and R. S. Thorne, Parton distributions in the LHC era: MMHT 2014 PDFs, Eur. Phys. J. C **75**, 204 (2015).
[87] Tie-Jiun Hou *et al.*, New CTEQ global analysis of quantum chromodynamics with high-precision data from the LHC, Phys. Rev. D **103**, 014013 (2021).
[88] G. Bevilacqua, H. B. Hartanto, M. Kraus, and M. Worek, Off-shell top quarks with one jet at the LHC: A comprehensive analysis at NLO QCD, J. High Energy Phys. 11 (2016) 098.
[89] Matteo Cacciari, Gavin P. Salam, and Gregory Soyez, The anti-k_t jet clustering algorithm, J. High Energy Phys. 04 (2008) 063.
[90] Matteo Cacciari and Gavin P. Salam, Dispelling the N^3 myth for the k_t jet-finder, Phys. Lett. B **641**, 57 (2006).

[91] Matteo Cacciari, Gavin P. Salam, and Gregory Soyez, FastJet user manual, Eur. Phys. J. C **72**, 1896 (2012).

[92] D. de Florian *et al.* (LHC Higgs Cross Section Working Group), Handbook of LHC Higgs cross sections: 4. Deciphering the nature of the Higgs sector, Report No. CERN-2017-002-M, 2017.

[93] Federico Buccioni, Stefan Kallweit, Stefano Pozzorini, and Max F. Zoller, NLO QCD predictions for $t\bar{t}b\bar{b}$ production in association with a light jet at the LHC, J. High Energy Phys. 12 (2019) 015.

[94] Giuseppe Bevilacqua, Huan-Yu Bi, Heribertus Bayu Hartanto, Manfred Kraus, Michele Lupattelli, and Malgorzata Worek, $t\bar{t}b\bar{b}$ at the LHC: On the size of corrections and b-jet definitions, J. High Energy Phys. 08 (2021) 008.

[95] Giuseppe Bevilacqua, Huan-Yu Bi, Heribertus Bayu Hartanto, Manfred Kraus, Michele Lupattelli, and Malgorzata Worek, $t\bar{t}b\bar{b}$ at the LHC: On the size of off-shell effects and prompt b-jet identification, arXiv:2202.11186.